Excited state absorption spectroscopy of ZBLAN:Ho^{3+} glass—experiment and simulation

2008 J. Phys.: Condens. Matter 20 155201

(http://iopscience.iop.org/0953-8984/20/15/155201)

J. Phys.: Condens. Matter **20** (2008) 155201 (11pp) doi:10.1088/0953-8984/20/15/155201

Excited state absorption spectroscopy of ZBLAN:Ho^{3+} glass—experiment and simulation

D Piatkowski[1,4], K Wisniewski[1,2], M Rozanski[1], Cz Koepke[1], M Kaczkan[3], M Klimczak[3], R Piramidowicz[3] and M Malinowski[3]

[1] Institute of Physics, Nicolaus Copernicus University, Grudziądzka 5/7, 87-100 Toruń, Poland
[2] Institute of Experimental Physics, University of Gdańsk, Wita Stwosza 57, 80-952 Gdańsk, Poland
[3] Institute of Microelectronics and Optoelectronics, Koszykowa 75, 00-662 Warsaw, Poland

E-mail: dapi@fizyka.umk.pl

Received 4 December 2007, in final form 7 February 2008
Published 25 March 2008
Online at stacks.iop.org/JPhysCM/20/155201

Abstract
The excited state absorption (ESA) spectra of ZBLAN glass activated by trivalent holmium ions have been measured in a wide spectral range (550–1750 nm) and simulated using such theoretical tools as the Judd–Ofelt formalism and McCumber theory of stimulated emission. We also propose a systematic approach for prediction of various types of up-conversion mechanisms in a given type of material. Experimental results on ESA up-conversion processes in ZBLAN:Ho^{3+} under red and infrared laser excitation, which confirm theoretical analysis, are presented. The optical linewidths were studied using high resolution laser spectroscopy at low temperatures and the existence of different crystallographic sites for Ho^{3+} ions was revealed.

(Some figures in this article are in colour only in the electronic version)

1. Introduction

In recent years visible and ultraviolet solid state lasers have attracted much attention due to the rapid growth of applications requiring short wavelength sources, such as full-color displays, optical data storage and biomedical instruments. Among various investigated systems, rare-earth-doped low phonon glasses have been reported as promising media for fiber and planar optical amplifiers and lasers [1]. From the energy level diagram of Ho^{3+} it could be observed that this ion has several high lying metastable levels, that can give rise to transitions at various wavelengths in the visible and ultraviolet region [2]. Up-conversion excitation of these high energy states could be obtained using multi-photon processes such as excited state absorption, energy transfer and, under certain conditions, combination of the above two mechanisms, which is called photon avalanche (PA).

In holmium compounds, the intense green emission centered at about 550 nm is associated with the $^5S_2$, $^5F_4 \rightarrow {}^5I_8$ transition. Continuous wave, green up-conversion lasing has been demonstrated in Ho^{3+} doped ZBLAN glass fibers pumped with red light in the 645 nm range, including InGaAlP laser diode pumping [3, 4]. Quite recently, gain and saturation intensity of the green up-conversion ZBLAN:Ho^{3+} amplifier and laser have been measured [5]. It should be noticed that in fiber geometry due to the waveguide effect and important interaction length, up-conversion mechanisms are enhanced. In ZBLAN:Ho^{3+}, up-converted luminescence from $^5S_2$, $^5F_4$ levels was also observed under excitation at different infrared wavelengths in the 720–770 nm, 880–920 nm and 960–990 nm spectral ranges [6, 7]. In most cases, the mechanism which generates the $^5S_2$, $^5F_4$ emission is ESA, because long lived $^5I_7$ (∼12 ms) and $^5I_6$ (∼3 ms) metastable states act as good population reservoirs and allow a high density of excited ions to be created. On the other hand, Rakov *et al* [8] reported results which show a strong evidence of energy transfer between holmium ions in fluoroindate glass excited by a pulsed laser operating at 640 nm. Moreover, under certain excitation wavelengths like 590, 750 and 840 nm, the photon avalanche mechanism based on ESA from the $^5I_7$, and $^5I_6$ states has been detected [9–12]. In addition, various blue and ultraviolet

[4] Author to whom any correspondence should be addressed.

emissions originating from the $^3D(1)_3$ and $^5G_4$ levels have been also observed in Ho^{3+}-doped glasses under visible and infrared excitation [8, 13, 14]. An intense white light has been observed under NIR excitation at about 750 nm in the Ho^{3+}-doped fluoride nanophase glass ceramic, which was due to strong photon avalanche emissions in the three primary colors [15]. Finally, ultraviolet signals were also recorded upon the same excitation conditions. Thus, within the Ho^{3+} ion, three possible non-exclusive mechanisms are responsible for population of the high lying emitting levels: excited state absorption, energy transfer and photon avalanche.

In this paper we investigate experimentally and theoretically the excited state absorption spectra of ZBLAN:Ho^{3+} glass in order to precisely assign observed up-converted emissions and to predict new ones. We also present up-converted luminescence excitation spectra which are compared with ESA measurements and calculations.

The composition of the ZBLAN glass used in the experiment was $53ZrF_4$:$20BaF_2$:$4LaF_3$:$3AlF_3$:$20NaF$. We concentrated on three bulk samples, containing 0.25, 1 and 2.5 mol% of holmium. The samples were developed and produced by Fiber Labs Co., Japan.

2. Experimental setup

Ground state absorption (GSA) spectra of ZBLAN:Ho^{3+} glasses were measured at room temperature by a Perkin-Elmer Lambda 2 UV–VIS spectrometer and by an Oriel MS125/InstaSpec II system with resolution better than 0.5 nm.

Emission and excitation spectra were measured using continuous wave (CW) as well as pulsed excitation. CW excitation in the blue-green region was achieved by an ILA-120 3 W argon ion laser. For infrared excitation, an argon laser (Coherent Innova 300, 10 W) pumped Ti-sapphire laser (Coherent 890 ring laser), tunable from 730 to 990 nm, or a Spectra 380 tunable dye laser operating with Rhodamine 6G dye, was used. Selectively excited spectra were measured using a pulsed dye laser operating with Coumarine 153 pumped by the third harmonic of a Continuum Nd:YAG laser. The dye laser has a linewidth of about 0.2 cm^{-1} and gives pulses of 10 ns. Sample cooling was provided by a closed cycle He optical cryostat, which allowed the temperature to be varied between 10 and 300 K. The spectra were recorded using a Jobin-Yvon or GDM 1000 monochromator with dispersion of 8 Å mm^{-1} and detected by an EMI 9789 or RCA C 31034-02 cooled AsGa photomultiplier. Data acquisition was obtained using a PAR 162 boxcar averager, SR 400 photon counting system or SR 510 lock-in amplifier controlled with a PC.

Excited state absorption measurements were performed by the pump and probe CW technique. The experimental setup, similar to those described in other publications [16–18], is shown in figure 1. The excitation beam was a 0.5 W, 488 nm line of an argon ion laser. The pump beam was modulated by a mechanical chopper at low frequency ($\nu_{pump} \sim 10$ Hz). Very stable choppers, Terahertz Technologies Inc. model C-995, were used in the experiment. The probe beam was provided by a stabilized 250 W tungsten–halogen lamp and was modulated at high frequency ($\nu_{probe} \sim 1$ kHz). Good

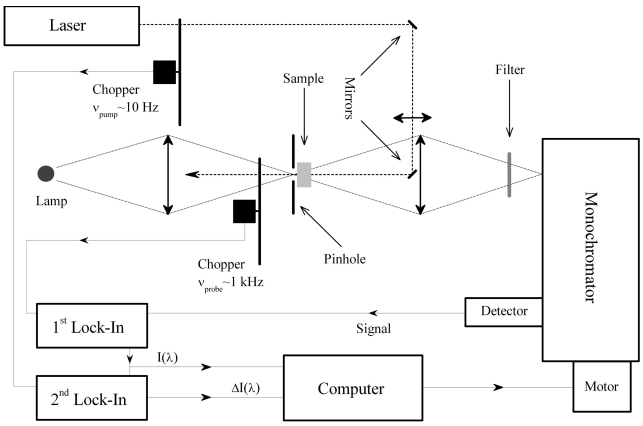

Figure 1. Experimental setup for CW pump–probe measurements.

overlap between the probe and pump beams was ensured by a pinhole and perfectly centered optics (cage system, Thorlabs). Since self-defocusing [19] under a strongly focused laser beam was observed in ZBLAN glass, a non-standard pinhole (600–700 μm) was used in the experiment, instead of the 150 μm usually applied. PIN photodiodes, Si (550–1100 nm) and InGaAs (1100–1800 nm), served as detectors, with direct anode current output, behind a 0.4 m prism monochromator. The resolution was 1 nm in the VIS range and 2 nm in the NIR. Differences in the light intensities transmitted through the sample with and without pump excitation $\Delta I(\lambda)$, together with the intensity $I(\lambda)$ transmitted through the unpumped sample, were measured simultaneously by a cascade of two DSP lock-in amplifiers (Signal Recovery 7265). The transmitted intensity was measured by the first lock-in (time constant 5 ms), where the high frequency chopper provided the reference. The output signal was also accumulated by a computer and analyzed by the second lock-in amplifier (time constant 5 s), where the difference intensity signal was measured. The signal in the second lock-in was maximized (zeroed phase shift) at the ESA peak, according to the transition $^5I_7 \rightarrow {}^5F_5$.

3. Ground state absorption—calculations

The ground state absorption spectrum of the 2.5 mol% ZBLAN:Ho^{3+} sample was measured in the range from 300 to 1200 nm and is shown in figure 2 (solid line). The spectrum shows several inhomogeneously broadened absorption bands, which were precisely assigned. The experimental energy levels were estimated from the barycentres of the absorption peaks and used for calculations (22 experimental points). The electronic energy levels were calculated in the framework of the free ion approximation by diagonalizing the energy matrix of the Hamiltonian of the Ho^{3+} ion [20, 21]:

$$H = E_{AVG} + \sum_{k=2,4,6} F^k f_k + \zeta A_{SO} + \alpha L(L+1) + \beta G(G_2) + \gamma G(R_7) + \sum_{\substack{i=2,3,4 \\ 6,7,8}} T^i t_i + \sum_{k=2,4,6} P^k p_k + \sum_{l=0,2,4} M^l m_l. \quad (1)$$

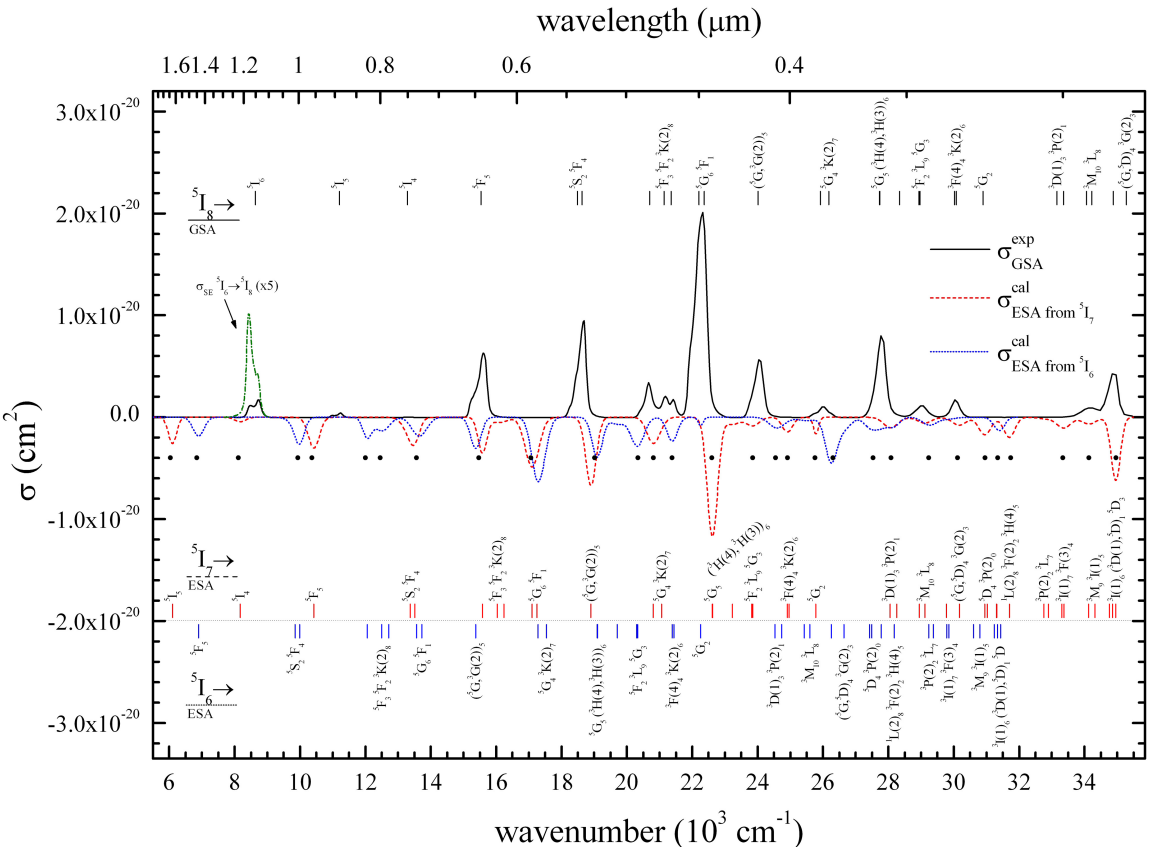

Figure 2. Spectra of experimental GSA (solid) and calculated ESA (dashed—from $^5I_7$, dotted—from $^5I_6$) cross sections along with assignments. Heavy dots denote possible channels of excitation of up-converted emission.

Table 1. Calculated energy parameters.

Parameter	Value	±	Parameter/ constant
E_{AVG}	48 410	39	P
F^2	96 246	273	P
F^4	67 252	467	P
F^6	46 803	249	P
ζ	2 149	9	P
α	017.2	—	C
β	−621	—	C
γ	2092	—	C
T^2	300	—	C
T^3	37	—	C
T^4	98	—	C
T^6	−316	—	C
T^7	440	—	C
T^8	372	—	C
P^2	523	—	C
P^4	392	—	C
P^6	262	—	C
M^0	3.0	—	C
M^2	1.68	—	C
M^4	1.14	—	C

Five parameters, representing the average energy of the configuration E_{AVE}, electron repulsions F^2, F^4, F^6 and the spin–orbit interaction ζ were freely varied. The remaining parameters, representing the two- and three-body configuration interactions and other magnetic interactions, were treated as constants for a given ion (Ho^{3+}) and taken from Carnall *et al* [2]. Software supplied by courtesy of Professor M.F. Reid (University of Canterbury, Christchurch, New Zealand) was used to evaluate the energy parameters. The best agreement between experimental and calculated energies was obtained for parameters listed in table 1. The root mean square deviation between the experimental and calculated energies was 57 cm^{-1}. Experimental and calculated energy levels are listed in table 2.

Experimental oscillator strengths of the transitions from the ground state to the excited states of the $4f^{10}$ configuration were evaluated from the GSA spectrum (17 experimental points) using the relation

$$f_{exp} = \frac{4\varepsilon_0 m_e c^2}{e^2} \int \sigma(\tilde{\nu})\, d\tilde{\nu} \qquad (2)$$

where σ is the cross section for ground state absorption, ε_0 is the vacuum permittivity, m_e is the rest mass of an electron, c is the velocity of light and e is the charge of an electron (in Coulombs). The concentration of holmium ions was 4.56×10^{20} cm^{-3} and the refractive index used in calculations was $n = 1.5$.

The electric-dipole oscillator strength between the levels of a $4f^n$ configuration is determined by at most three Judd–Ofelt intensity parameters and by the squares of the reduced

Table 2. Energy levels, GSA and ESA transition intensities and line widths.

Level	E_{exp} (cm^{-1})	E_{cal} (cm^{-1})	f_{exp} for group ($\times10^{-6}$)	f_{cal} for level ($\times10^{-6}$)	f_{cal} for group ($\times10^{-6}$)	Transition energy (cm^{-1})	f_{cal} for level ($\times10^{-6}$)	Transition energy (cm^{-1})	f_{cal} for level ($\times10^{-6}$)	Γ HWHM (cm^{-1})
$^5I_8$	0	45		↓ GSA ↓		↓ ESA from $^5I_7$ ↓				—
$^5I_7$	—	5113	—	1.27	1.27			↓ ESA from $^5I_6$ ↓		—
$^5I_6$	—	8636	0.73	0.94	0.94	3 524	1.17			220
$^5I_5$	11 191	11 211	0.15	0.17	0.17	6 098	0.93	2 574	0.83	150
$^5I_4$	13 329	13 285	0.02	0.02	0.02	8 172	0.22	4 649	0.62	200
$^5F_5$	15 569	15 536	2.63	2.41	2.41	10 424	1.46	6 900	0.89	200
$^5S_2$	18 424	184 85	3.50	0.57	3.26	13 372	0.93	9 848	0.33	250
$^5F_4$	18 660	18 626		2.69		13 513	0.59	9 990	0.91	170
$^5F_3$	20 666	20 693		1.05		15 580	1.34	12 057	0.75	160
$^5F_2$	21 172	21 141	2.20	0.64	2.38	16 028	0.21	12 505	0.77	250
$^3K(2)_8$	21 448	21 350		0.69		16 238	0.16	12 714	0.07	277
$^5G_6$	22 255	22 207	10.5	10.5	10.5	17 095	2.82	13 571	0.58	250
$^5F_1$	—	22 363		—		17 250	0.16	13 727	0.63	250
$(^5G, ^3G(2))_5$	24 034	24 015	2.33	2.17	2.17	18 903	3.06	15 379	1.4	190
$^5G_4$	25 783	25 917	0.48	0.29	0.47	20 804	1.37	17 280	3.36	227
$^3K(2)_7$	26 038	26 175		0.18		21 063	0.12	17 539	0.30	186
$^5G_5$	—	27 729		1.08		22 617	4.82	19 093	1.75	190
$(^3H(4), ^3H(3))_6$	27 779	27 739	3.41	2.11	3.21	22 626	0.54	19 102	0.04	190
$^5F_2$	—	28 343		0.02		23 230	0.42	19 706	0.40	250
$^3L_9$	—	28 931	0.57	0.77	0.83	23 818	0.07	20 295	0.17	240
$^5G_3$	29 017	28 965		0.06		23 852	0.42	20 329	1.47	240
$^3F(4)_4$	30 054	30 024	0.60	0.65	0.68	24 911	0.64	21 387	1.04	190
$^3K(2)_6$	—	30 075		0.03		24 963	0.03	21 439	0.05	240
$^5G_2$	—	30 896	0.003	0.003	0.003	25 784	0.37	22 260	0.18	95
$^3D(1)_3$	—	33 162		0.01		28 049	0.58	24 526	0.47	250
$^3P(2)_1$	—	33 366		—		28 253	0.08	24 730	0.23	250
$^3M_{10}$	—	34 057	2.60	0.80	3.00	28 944	0.03	25 421	0.21	360
$^3L_8$	34 287	34 228		0.07		29 116	0.33	25 592	0.07	250
$(^5G, ^5D)_4$	34 886	34 885		2.10		29 772	0.01	26 249	2.18	210
$^3G(2)_3$	—	35 282		0.02		30 169	0.47	26 646	0.67	250
$^5D_4$	36 047	36 065		1.73		30 952	0.91	27429	0.40	220
$^3P(2)_0$	—	36 133		—		31 020	—	27 497	0.09	250
$^1L(2)_8$	—	36 418	1.88	0.04	1.83	31 305	0.02	27 781	0.12	250
$^3F(2)_2$	—	36 423		0.02		31 310	0.004	27 787	0.44	250
$^3H(4)_5$	—	36 815		0.04		31 702	0.95	28 179	0.39	200
$^3P(2)_2$	—	37 873		0.00		32 760	0.06	29 236	0.39	250
$^3L_7$	—	38 008	0.30	0.03	0.24	32 895	0.03	29 371	0.10	250
$^3I(1)_7$	—	38 422		0.18		33 309	0.13	29 785	0.05	250
$^3F(3)_4$	38 475	38 490		0.03		33 377	0.52	29 853	0.06	250
$^3M_9$	—	39 236		0.06		34 123	0.37	30 600	0.01	250
$^3I(1)_5$	—	39 433		0.01		34 321	0.04	30 797	0.006	250
$^3I(1)_6$	—	39 876	0.47	0.08	0.32	34 764	0.04	31 240	0.14	144
$(^3D(1), ^5D)_1$	—	39 970		0.00		34 857	0.05	31 334	0.01	250
$^5D_3$	40 085	40 069		0.17		34 957	2.43	31 433	0.46	165
$^5D_4$	41 565	41 612	—	1.85	1.85	36 499	1.01	32 976	0.35	—

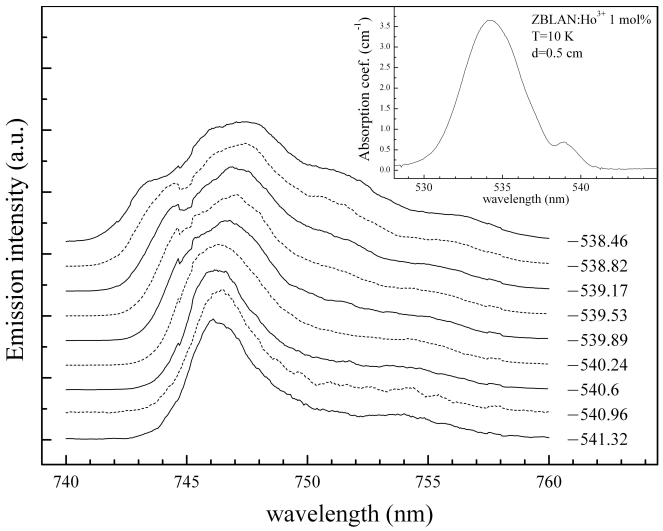

Figure 3. Selectively excited emission spectra, corresponding to the $^5S_2 \rightarrow {}^5I_7$ transition of ZBLAN:Ho^{3+} glass at 10 K. The inset presents the low temperature absorption spectrum showing the $^5I_8 \rightarrow {}^5S_2$,$^5F_4$ profile.

matrix elements of the unit tensor operator $U^{(\lambda)}$ with ranks 2, 4 and 6 [22, 23]:

$$f_{\mathrm{cal}} = \frac{8\pi^2 m_e c\tilde{\nu}\chi}{3h(2J+1)} \times \sum_{\lambda=2,4,6} \Omega_\lambda \left|\left\langle 4f^n \gamma'[S'L']J' \left\| U^{(\lambda)} \right\| 4f^n \gamma[SL]J \right\rangle\right|^2, \quad (3)$$

where $\tilde{\nu}$ is the mean energy for the transition (in cm^{-1}), χ is the local field correction, approximated for absorption by $(n^2+2)^2/9n$, h is the Planck constant and J is the total angular momentum of the initial state in the transition [24]. The functions in the matrix element are expressed in the intermediate coupling scheme. The intermediate coupling coefficients were found by diagonalizing the energy matrix of the Ho^{3+} ion. The reduced matrix elements of the unit tensor operators were published by Nielson and Koster [25]. The Judd–Ofelt intensity parameters were determined by minimizing the sum of the squares of the differences between the experimental and calculated oscillator strengths. For the 2.5 mol% ZBLAN:Ho^{3+} sample, the following intensity parameters were established:

$$\Omega_2 = (2.46 \pm 0.22) \times 10^{-20}\ \mathrm{cm}^2,$$

$$\Omega_4 = (2.02 \pm 0.39) \times 10^{-20}\ \mathrm{cm}^2,$$

$$\Omega_6 = (1.71 \pm 0.24) \times 10^{-20}\ \mathrm{cm}^2$$

and are in good agreement with those published by Görller-Walrand and Binnemans for the ZBLAN:Ho^{3+} system [26, 27]. The root mean square deviation between the experimental and calculated oscillator strengths was 1.7×10^{-7}. Experimental and calculated oscillator strengths are compared in table 2.

4. Linewidths

4.1. Experiment

Optical transitions of ions in glasses are inhomogeneously broadened as a consequence of site to site variations of the local crystal fields. The absence of structural restrictions on the active ion site in glass results in the 'averaged' wide spectrum, which is strongly broadened as compared to most crystals, and where Stark splitting and resulting line structure is difficult to resolve. This situation is advantageous for obtaining a flat gain spectrum of glass fiber amplifiers for optical telecommunication (wavelength division multiplexing) [28, 29]. However, reports concerning linewidth studies in ZBLAN glass are quite limited [30, 31]. Recently, optical spectra of RE^{3+} doped ZBLAN were successfully simulated [32–34]. A still controversial issue is the existence of different crystallographic sites for luminescent ions. Observations of two sites were reported for europium [35] and erbium [36] ions in fluoride glasses.

We investigated a 1 mol% ZBLAN:Ho^{3+} sample. A narrow-band tunable laser was used to excite selectively into the $^5I_8 \rightarrow {}^5S_2$ absorption line when nonresonant $^5S_2 \rightarrow {}^5I_7$ emission was recorded. We also studied excitation spectra for various emission lines. Part of the absorption spectrum acquired at 10 K is shown in the inset of figure 3. The absorption spectrum can be well fitted using the decomposition of two Gaussian lines. This gives us the low temperature energy value of the center of the $^5F_4$ and $^5S_2$ levels to be 18 714 cm^{-1} (534.35 nm) and 18 545 cm^{-1} (539.22 nm) respectively, together with the corresponding 10 K linewidths of 132 cm^{-1} and 53.4 cm^{-1}. After selective, narrow line excitation around 539 nm, low temperature emission spectra of ZBLAN:Ho^{3+} glass were registered and are shown in figure 3. As could be seen, Stark components of the $^5S_2 \rightarrow {}^5I_7$ are not well resolved, but excitation-wavelength-dependent lineshape, energy shift and remarkable narrowing of the emission as the excitation energy decreases within the $^5I_8 \rightarrow {}^5S_2$ absorption spectrum have been obtained. Two distinct lineshapes can be observed: for excitation wavelength shorter than about 540 nm, emission profiles are wider with visible features at 744 nm and 751 nm; excitation wavelengths longer than 540 nm resulted in simpler and much narrower emission centered at 746.5 nm. The smallest linewidth (FWHM) observed at 10 K under 541.32 nm excitation was 62 cm^{-1}. This suggests the presence of two different sites for holmium ions. However, the fluorescence decays measured after selective excitation have the same temporal dynamics, with the long time decay constant of 198 μs.

4.2. Calculations and modeling

In our calculations, room temperature was assumed to omit the necessity of deciding which site is dominating in the simulated spectra. For estimation of the room temperature linewidths of the absorption spectra, a procedure similar to that presented by Binnemans *et al* [27] was used. This procedure was successfully applied by us for Nd^{3+}-doped glass and reported

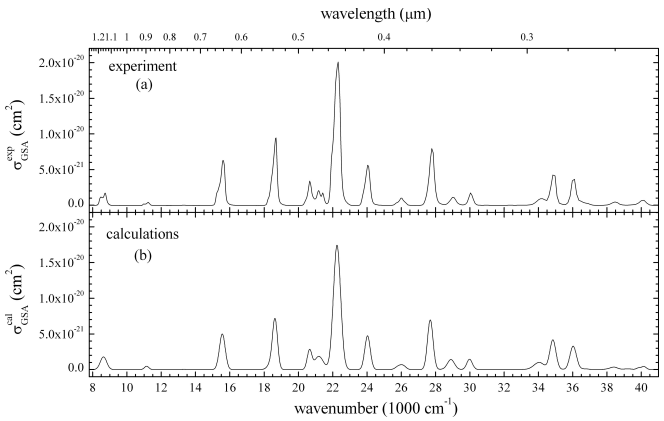

Figure 4. Experimental (a) and reproduced (b) GSA spectra.

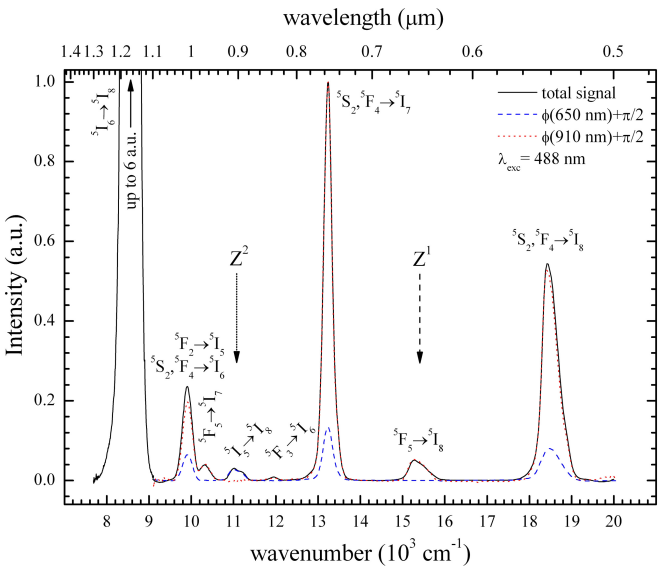

Figure 5. Emission spectra of the ZBLAN:Ho^{3+} sample measured using phase sensitive detection.

in a previous paper [37]. In the present work, the linewidths for the ZBLAN:Ho^{3+} system, determined in the same way, are used for the ESA spectrum simulations.

Inhomogeneously broadened absorption peaks in a glass matrix are described by the Gaussian function:

$$G_i(\tilde{\nu}) = \sqrt{\frac{\ln 2}{\pi \Gamma_i^2}} \exp\left(-\Gamma_i^{-2}(\tilde{\nu} - \tilde{\nu}_{0i})^2 \ln 2\right) \tag{4}$$

as a superposition of many Lorentzians, where Γ is the half-width at half-maximum (HWHM) and $\tilde{\nu}_0$ is the peak center (all in cm^{-1}). The above function is normalized ($\int G_i(\tilde{\nu})\, d\tilde{\nu} = 1$) and then multiplied by f_{cal} to express the intensity of the particular transition in the units of cross section:

$$\sigma^{cal}(\tilde{\nu}) = \frac{e^2}{4\varepsilon_0 m_e c^2} \sum_{i=1}^{p} f_{i_{cal}} G_i(\tilde{\nu}), \tag{5}$$

and relates to the p transitions in the band. Since $f_{i_{cal}}$ and $\tilde{\nu}_{0i}$ are known from calculations, Γ_i can be treated as adjustable parameters to fit the GSA spectrum. An estimated set of the Judd–Ofelt intensity parameters, energy parameters and gamma parameters can by used for the complete GSA spectrum reproduction or ESA spectrum simulation [38]. Reproduced and experimental ground state absorption spectra are compared in figure 4. The evaluated Γ_i parameters are listed in table 2.

5. Luminescence

The emission spectrum of the ZBLAN:Ho^{3+} sample was measured using a slightly reorganized excited state absorption experimental setup, based on one lock-in amplifier and argon ion laser working at 488 nm, modulated at a frequency of about 40 Hz. To distinguish between emissions from different initial states, phase sensitive detection (PSD) has been applied [39]. The solid line in figure 5 (total signal, without PSD) presents several emission lines in the examined spectral range (500–1400 nm). Then signal was maximized (zeroed phase shift) at 650 nm (Z^1 point in figure 5) and the quadrature (signal shifted by $\pi/2$) was registered. The obtained spectrum (dashed line), normalized at the Z^2 line (and vice versa), presents no transitions at 650 and 970 nm, which proves that they originate from the same level. We assigned these lines to the $^5F_5 \rightarrow {}^5I_8$ and $^5F_5 \rightarrow {}^5I_7$ transitions respectively. When signal was maximized at 910 nm, the spectrum obtained in quadrature presents all remaining lines. Therefore, we ascribed only this line to the transition from $^5I_5$ level ($^5I_5 \rightarrow {}^5I_8$). The remaining, intense transitions peaking at 540, 755 and 1010 nm originate from thermalized $^5S_2$ and $^5F_4$ levels and lead to the $^5I_{8,7,6}$ levels respectively. Finally, we can note very intense emission peaking at 1170 nm ($^5I_6 \rightarrow {}^5I_8$), which is over six times stronger than the $^5S_2$, $^5F_4 \rightarrow {}^5I_7$ transition. Comparing the calculated Einstein's coefficients for these transitions, $A_{^5I_6 \rightarrow {}^5I_8} = 150\ s^{-1}$, $A_{^5S_2 \rightarrow {}^5I_7} = 750\ s^{-1}$ and $A_{^5F_4 \rightarrow {}^5I_7} = 270\ s^{-1}$, it is obvious that population of the $^5I_6$ level is over an order of magnitude larger than that of other, higher levels. Therefore only $^5I_6 \rightarrow {}^5I_8$ emission was considered in the simulation of the ESA experiment. The stimulated emission (SE) cross section was calculated from the Füchtbauer–Ladenburg equation,

$$\sigma_{SE} = \frac{1}{8\pi n^2 c} \frac{\beta}{\tau_R} \frac{\lambda^5 I(\lambda)}{\int \lambda I(\lambda)\, d\lambda}, \tag{6}$$

which is compatible with the McCumber approach, and the result is shown in figure 2 (dash–dotted line).

6. Excited state absorption

6.1. Experiment

Using the setup described earlier, an ESA experiment was performed. Assuming that A is the amplification constant of the second lock-in, measured signals can be described by the

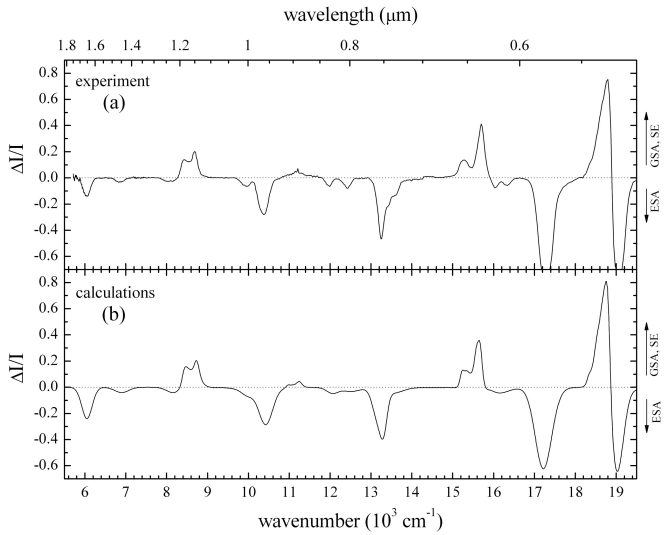

Figure 6. Experimental (a) and calculated (b) EST spectra.

approximated expression [40]

$$\frac{\Delta I(\lambda)}{I(\lambda)} = AL\left(N^*\sigma_{\mathrm{GSA}}(\lambda) + \sum_i N_i\left(\sigma_{\mathrm{SE}_i}(\lambda) - \sigma_{\mathrm{ESA}_i}(\lambda)\right)\right), \tag{7}$$

where N^* is the total excited population density, N_i is the ith excited level population density ($\Sigma N_i = N^*$) and L is the length of the sample (5 mm). In the experiment, GSA, SE and ESA transitions can appear simultaneously, sometimes in the same spectral range. In this paper we call such a spectrum the excited state transmission (EST), to distinguish it from the pure excited state absorption spectrum where GSA and SE transitions do not occur. Pay attention to the term $N^*\sigma_{\mathrm{GSA}}$ in equation (7). It is of the same sign as $N_i\sigma_{\mathrm{SE}}$ and describes the GSA (bleaching) transitions. The measured EST spectrum is shown in figure 6(a).

6.2. Calculations and modeling

Estimation of the ESA spectrum from the experimental data is often difficult or even impossible. For some systems, where N_i represents the entire excited population ($N_i = N^*$) and no SE and GSA transitions occur, σ_{ESA} can be calculated directly from the EST spectrum using equation (7). However, in most cases N^* is distributed among several levels and σ_{ESA} cannot be simply evaluated.

One can try to calculate the ESA spectrum directly. When transition energies are known from the energy levels calculations, the ESA oscillator strengths can be simply computed using the Judd–Ofelt approach. Unfortunately, the linewidths of such transitions are unknown. Therefore we calculated the excited state absorption spectrum utilizing the same Γ parameters for the ESA transitions as those evaluated from the ground state absorption spectrum for the identical final states. Such simplification seems to be reasonable under the assumption that all transitions, from the ground or excited state, take place from the lowest sublevel of the particular state. Then mostly the final states determine linewidths. The postulated approach is successfully verified by the EST spectrum simulation in the following manner.

The excited state absorption spectra ($\sigma_{\mathrm{ESA}}^{\mathrm{cal}}$) originating from the $^5I_7$ and $^5I_8$ levels were calculated from equation (5) for oscillator strengths, transition energies and linewidths listed in table 2. These spectra are shown in figure 2 (dashed—ESA starting from $^5I_7$, dotted—ESA starting from $^5I_6$). The total excited population density N^*, required for modeling, can be evaluated from the bleaching features which do not overlap SE and/or ESA. Unfortunately, most of the GSA transitions compete with ESA in the broad spectral range. Only one transition, ascribed to $^5I_8 \rightarrow {}^5I_5$, can be recognized as separated from other transitions. Using the expression [16]

$$N^* = \frac{\int \Delta I(\lambda)/I(\lambda)\,\mathrm{d}\lambda}{AL\int \sigma_{\mathrm{GSA}}\,\mathrm{d}\lambda}, \tag{8}$$

the density of the total excited population was estimated to be 1×10^{17} cm^{-3}. However, because of the low intensity of the $^5I_8 \rightarrow {}^5I_5$ transition, the estimated N^* value can be treated only as a reasonable approximation.

The experimental cross sections for GSA and SE, as well as the calculated cross section for ESA occurring from $^5I_7$ and $^5I_6$ states, as presented in figure 2, were used to calculate the EST spectrum using equation (7). Good agreement between the measured and calculated EST spectra was obtained when assuming that $N(^5I_7) = 0.76N^*$ and $N(^5I_6) = 0.18N^*$. This proves that ESA starting from $^5I_7$ and $^5I_6$ levels dominates in the experiment. However, transitions starting from other, also populated excited levels are possible. The calculated EST spectrum is presented in figure 6(b) and confirms that the ESA spectrum, calculated with the Judd–Ofelt theory and with evaluated Γ parameters, simulates the experimental excited state transmission spectrum correctly.

6.3. Confrontation of the ESA and excitation spectra

Most of the ESA transitions considered here end up in the excitation of the $^5S_2$,$^5F_4$ metastable levels of holmium ions. Green, up-converted fluorescence of the Ho^{3+} ion, corresponding to the $^5S_2$,$^5F_4 \rightarrow {}^5I_8$ transition, was observed after red and infrared excitation in the 580–650 nm, 720–770 nm, 880–920 nm and 960–990 nm spectral ranges. Figure 7 shows the excitation spectrum of the green emission together with the GSA spectrum and identifies the observed and calculated ESA transitions. In addition to the strong green signal centered at about 550 nm, we also observed a weak emission in the blue region (490 nm), resulting from the $^5F_3 \rightarrow {}^5I_8$ transition and red emission (645 nm) from the excited $^5F_5$ state to the ground $^5I_8$ state. It was found that the relative intensities of these lines depend on the excitation wavelength. From our earlier studies of YLF:Ho^{3+} crystals [41] and theoretical analysis presented here, it turns out that at several wavebands GSA and ESA transitions from low excited states of holmium ions overlap. Most of the presented up-conversion excitation spectra are compatible with theoretically determined ESA transitions shown in figure 2.

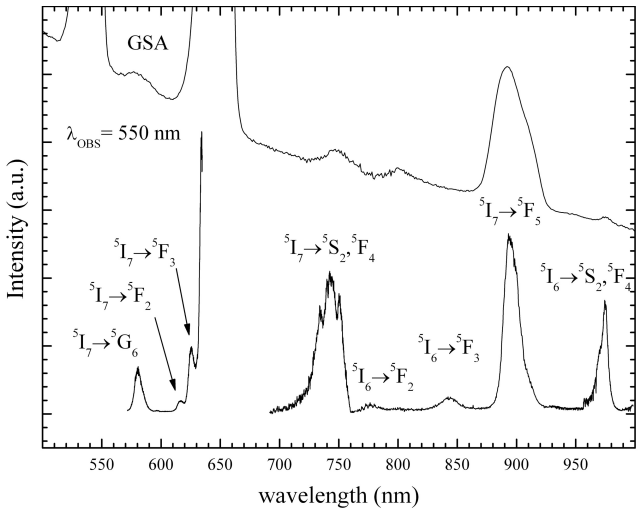

Figure 7. Room temperature excitation spectrum of the green up-converted luminescence together with the absorption spectrum of ZBLAN:Ho^{3+}.

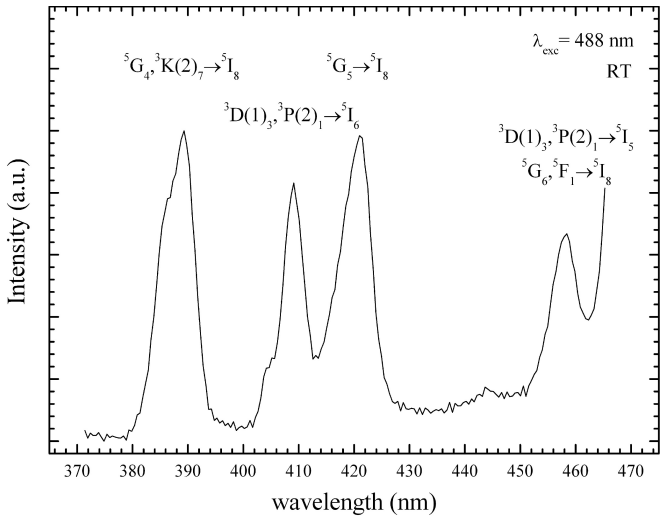

Figure 8. Up-converted luminescence under 488 nm laser excitation.

7. Up-conversion analysis

Based on the calculated cross sections for the ESA transitions as well as the experimental GSA spectrum, different excitation channels leading to the up-converted emissions can be recognized. Analyzing figure 2, one can see several wavelengths where σ_{GSA} and σ_{ESA} are peaking in the same spectral range. Such excitation wavelengths can lead to the up-converted emission (ESA type of up-conversion) under the assumption that the GSA transition populates $^5I_7$ and/or $^5I_6$ level(s). Then, the second photon is absorbed via excited state absorption and excites the high lying levels, from which the up-converted emission can occur. Another possible up-converted emission mechanism is photon avalanche. When the pump wavelength corresponds to the maximum of the ESA transition from a metastable level, whereas the ground state absorption is considerably lower or even absent, the photon avalanche phenomenon is expected to occur [42]. Of course, efficient cross relaxation energy transfer feeding the metastable level is also required. However, the spectral relationship between GSA and ESA transitions is also important and considered in this paper. Probable up-converted emission excitation channels are marked in figure 2 by heavy dots and listed in table 3. Some of them have already been demonstrated but most have not been reported until now.

We have attempted to excite our sample into some of the wavelengths indicated by the above analysis. First we used a 1 W, 488 nm argon ion laser beam to excite the 2.5 mol% ZBLAN:Ho^{3+} sample. The observed up-converted emission shows several lines assigned precisely in figure 8. The transitions originating from $^5G_4$, $^3K(2)_7$ and $^5G_5$ levels can be excited efficiently via ESA starting from $^5I_7$ and/or $^5I_6$. However, other lines peaking at 409 and 458 nm cannot be explained in this scheme. These up-converted emission lines originate from $^3D(1)_3$ and $^3P(2)_1$ levels and can be excited otherwise, via ESA starting from also populated $^5F_5$ level.

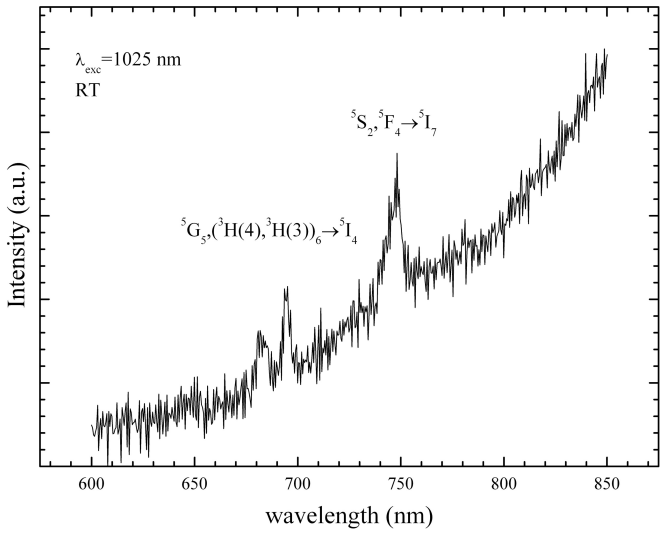

Figure 9. Up-converted luminescence under 1025 nm diode laser excitation.

Calculated oscillator strength for the $^5F_5 \rightarrow {}^5D_4$ transition is about 1.8×10^{-6} and its energy perfectly fits to the used argon laser line. We assigned these lines to the $^3D(1)_3$,$^3P(2)_1 \rightarrow {}^5I_6$ and $^3D(1)_3$,$^3P(2)_1 \rightarrow {}^5I_5$ transitions respectively. However, the line centered at 458 nm can be also assigned to the phonon-assisted $^5G_6$,$^5F_1 \rightarrow {}^5I_8$ transition, which proves our new results (paper under preparation).

We also used a 300 mW diode laser working at 1025 nm to explore $^5I_6 \rightarrow {}^5S_2$, $^5F_4$ transition. For this wavelength no ground state absorption occurs and therefore a photon avalanche mechanism is expected. The observed up-converted emission line peaking at 750 nm (figure 9) is a well defined $^5S_2$,$^5F_4 \rightarrow {}^5I_7$ transition. Two weaker lines centered at 690 nm cannot originate from these levels and rather a $^5G_5$, ($^3H(4)$, $^3H(3))_6 \rightarrow {}^5I_4$ transition should be considered here. Laser diode excitation of about 1025 nm also fits the

Table 3. Predicted up-converted emission excitation channels.

Pumping wavelength (nm)	Excitation channel		Mechanism	References
	1st step	2nd step		
1640	—	$^5I_7 \rightarrow {}^5I_5$	PA	
1450	—	$^5I_6 \rightarrow {}^5F_5$	PA	
1225	—	$^5I_7 \rightarrow {}^5I_4$	PA	
1002	—	$^5I_6 \rightarrow {}^5F_4$	PA	
960	—	$^5I_7 \rightarrow {}^5F_5$	PA	
830	—	$^5I_6 \rightarrow {}^5F_3$	PA	[12]
800	—	$^5I_6 \rightarrow {}^5F_2$	PA	
735	—	$^5I_7 \rightarrow {}^5S_2$ $^5I_6 \rightarrow {}^5G_6, {}^5F_1$	PA	[11, 12]
645	$^5I_8 \rightarrow {}^5F_5$	$^5I_7 \rightarrow {}^5F_3$ $^5I_6 \rightarrow ({}^5G, {}^3G(2))_5$	ESA	[4, 14]
585	—	$^5I_7 \rightarrow {}^5G_6$ $^5I_6 \rightarrow {}^5G_4$	PA	[9, 10]
525	$^5I_8 \rightarrow {}^5F_4$	$^5I_7 \rightarrow ({}^5G, {}^3G(2))_5$ $^5I_6 \rightarrow {}^5G_5$	ESA/PA	
491	$^5I_8 \rightarrow {}^5F_3$	$^5I_6 \rightarrow {}^5G_3$	ESA/PA	
480	$^5I_8 \rightarrow {}^5F_3$	$^5I_7 \rightarrow {}^5G_4$	ESA	
467	$^5I_8 \rightarrow {}^3K(2)_8$	$^5I_6 \rightarrow {}^3F(4)_4$	ESA	
442	$^5I_8 \rightarrow {}^5G_6$	$^5I_7 \rightarrow {}^5G_5$	ESA/PA	
419	$^5I_8 \rightarrow ({}^5G, {}^3G(2))_5$	$^5I_7 \rightarrow {}^5F_2, {}^5G_3$	ESA	
407	—	$^5I_6 \rightarrow {}^3D(1)_3$	PA	
401	—	$^5I_7 \rightarrow {}^3F(4)_4$	PA	
388	$^5I_8 \rightarrow {}^5G_4$	$^5I_7 \rightarrow {}^5G_2$	ESA	
380	$^5I_8 \rightarrow {}^3K(2)_7$	$^5I_6 \rightarrow {}^5G_4$	ESA/PA	
363	$^5I_8 \rightarrow ({}^3H(4), {}^3H(3))_6$	$^5I_6 \rightarrow {}^5D_4$	ESA	
356	$^5I_8 \rightarrow ({}^3H(4), {}^3H(3))_6$	$^5I_7 \rightarrow {}^3D(1)_3$ $^5I_6 \rightarrow {}^3F(2)_2, {}^3H(4)_5$	ESA	
342	$^5I_8 \rightarrow {}^3L_9$	$^5I_7 \rightarrow {}^3L_8$ $^5I_6 \rightarrow {}^3P(2)_2$	ESA	
332	$^5I_8 \rightarrow {}^3F(4)_4$	$^5I_7 \rightarrow {}^3G(2)_3$	ESA	
323	—	$^5I_7 \rightarrow {}^5D_4$	PA	
319	—	$^5I_6 \rightarrow {}^5D_3$	PA	
315	—	$^5I_7 \rightarrow {}^3H(4)_5$	PA	
300	—	$^5I_7 \rightarrow {}^3F(3)_4$	PA	
293	$^5I_8 \rightarrow {}^3M_{10}$	$^5I_7 \rightarrow {}^3M_9$	ESA	
286	$^5I_8 \rightarrow {}^5G_4$	$^5I_7 \rightarrow {}^5D_3$	ESA	

$^5S_2$,$^5F_4 \rightarrow {}^5F_2$ transitions, therefore the proposed assignment seems to be quite reasonable. Nevertheless, the presented up-converted emission under 1025 nm excitation requires more investigations, especially by registering up-converted luminescence intensity versus power of the pump beam.

We can show that 'inflection points' between the ESA and GSA features, seen in figure 2, are also attractive as excitation wavelengths. We have chosen a region 880–910 nm where a quite small GSA feature competes with the ESA. The 890 nm excitation band was studied in detail and the up-converted luminescence color differences, when slightly changing the excitation wavelength, were observed. After excitation at about 880–885 nm the luminescence observed by the naked eye was reddish (emission from the $^5F_5$ state dominated), and for longer wavelengths, excitation between 890 and 910 nm, the luminescence color was green (emission from the $^5S_2$, $^5F_4$ states dominated). This suggested that different up-conversion excitation processes are taking place, which could be analyzed with the energy scheme presented in figure 10. The investigated waveband corresponds to the direct $^5I_8 \rightarrow {}^5I_5$ transition as shown in figure 10. The 890–910 nm excitation is next resonant with the $^5I_5 \rightarrow {}^5F_1$ transition leading to efficient population of the $^5S_2$, $^5F_4$ levels, from which green emission is observed. For shorter excitation wavelengths, in the 880–885 nm range, the second step transition $^5I_5 \rightarrow {}^5F_1$ is no longer resonant and thus less intense. In this situation the $^5I_7 \rightarrow {}^5F_5$ process leading to red $^5F_5$ emission dominates. In between, there are efficient ESA transitions of the type $^5I_6 \rightarrow {}^5S_2$, $^5F_4$. In the up-conversion processes discussed above, $^5I_7$, $^5I_6$ and $^5I_5$ manifolds are involved as the intermediate states.

8. Conclusions

The results of the ESA spectra calculations, performed using the Judd–Ofelt approach, were successfully compared with the experiment. Based on the calculated spectra, more than ten up-converted emission excitation channels in ZBLAN:Ho^{3+} were suggested. Some of them have experimentally been proved to

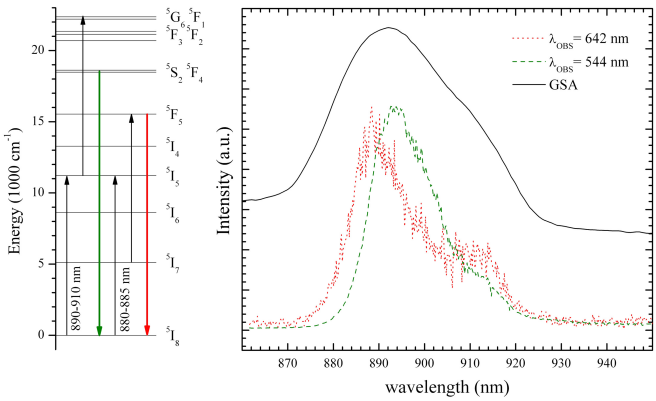

Figure 10. Excitation spectra of the green ($^5S_2$,$^5F_4 \rightarrow {}^5I_8$) and red ($^5F_5 \rightarrow {}^5I_8$) emissions of ZBLAN:$Ho^{3+}$ and the energy level diagram identifying excitation pathways.

be operative, some have not been considered until now. We have also demonstrated, that under 488 nm excitation, the ESA transitions from $^5I_7$ and $^5I_6$ levels dominate. However, ESA transitions originating from $^5I_5$, $^5F_5$ and $^5S_2$, $^5F_4$ levels should also be considered as valid for some excitation channels.

Acknowledgments

This work was supported by the Nicolaus Copernicus University (NCU) by local grants 377-F and 362-F and by the Grant of the NCU Rector, under number 517-F. KW was supported by the Polish Committee for Scientific Research (project PBZ/MEiN/01/2006/39). This work was also co-financed by the European Social Fund and the state budget under a project of the Regional Council of the Kujawsko-Pomorskie Province: 'Step into the future—scholarships for PhD students'. DP is very grateful to Professor MF Reid, University of Canterbury, Christchurch, New Zealand, for making it possible to use his software. The authors from IMiO gratefully acknowledge the support of the Laboratoire de Physico-Chimie des Matériaux Luminescents in Lyon where part of the excitation measurements were performed. The authors are grateful to the Fiber Labs Co., Japan, for supplying the samples.

References

[1] Funk S and Eden J G 1995 *IEEE J. Sel. Top. Quantum Electron.* **1** 784
[2] Carnall W T, Crosswhite H and and Crosswhite H M 1977 Energy level structure and transition probabilities of the trivalent lanthanides in LaF_3 *Argonne National Laboratory Report*
[3] Allain J Y, Monerie M and Poignant H 1990 *Electron. Lett.* **26** 261
[4] Funk D S and Eden J G 2001 *IEEE J. Quantum Electron.* **37** 980
[5] Mejia E B, Senin A A, Talmadge J M and Eden J G 2002 *IEEE Photon. Technol. Lett.* **14** 1500
[6] Wnuk A, Kaczkan M, Piramidowicz R, Mahiou R, Bertrand G, Joubert M-F and Malinowski M 2003 *Radiat. Eff. Defects Solids* **158** 469
[7] Yong G C, Bong J P and Kyong H K 2002 *Chem. Phys. Lett.* **354** 69
[8] Rakov N, Maciel G S, de Araujo Cid B and Messaddeq Y 2002 *J. Appl. Phys.* **91** 1272
[9] Liu G K, Chen Y H and Beitz J V 1999 *J. Lumin.* **81** 7
[10] Malinowski M, Wnuk A, Frukacz Z, Chadeyron G, Mahiou R, Guy S and Joubert M-F 2001 *J. Alloys Compounds* **323/324** 731
[11] Lahoz F, Martin I R, Guadalupe V L, Méndez-Ramos J, Rodríguez V D and Rodríguez-Mendoza U R 2004 *Opt. Mater.* **25** 209
[12] Lavín V, Lahoz F, Martín I R, Rodrıguez-Mendoza U R and Cáceres J M 2005 *Opt. Mater.* **27** 1754
[13] Tanimura K, Shinn M D, Sibley W A, Drexhage M G and Brown R N 1984 *Phys. Rev.* B **30** 2429
[14] Kowalska M, Klocek G, Piramidowicz R and Malinowski M 2004 *J. Alloys Compounds* **380** 156
[15] Lahoz F, Martín I R and Calvilla-Quintero J M 2005 *Appl. Phys. Lett.* **86** 051106
[16] Le Boulanger P, Doualan J L, Girard S, Margerie J and Moncorgé R 1999 *Phys. Rev.* B **60** 11380
[17] Wegner T and Petermann K 1989 *Appl. Phys.* B **49** 275
[18] Kück S, Osiac E and Sokólska I 2005 *J. Opt. Soc. Am.* B **22** 232
[19] Adam J L, Doualan J L, Griscom L, Girard S and Moncorgé R 1999 *J. Non-Cryst. Solids* **256–257** 276
[20] Morrison A and Leavitt R P 1982 *Handbook on the Physics and Chemistry of Rare Earths* vol 5 (Amsterdam: North-Holland) chapter 46
[21] Wybourne B G 1965 *Spectroscopic Properties of Rare Earths* (New York: Wiley)
[22] Judd B R 1962 *Phys. Rev.* **127** 750
[23] Ofelt G S 1962 *J. Chem. Phys.* **37** 511
[24] Carnall W T 1979 *Handbook on the Physics and Chemistry of Rare Earths* vol 3 (Amsterdam: North-Holland) chapter 24
[25] Nielson C W and Koster G F 1963 *Spectroscopic Coefficients for the p^n, d^n and f^n Configurations* (Cambridge, MA: MIT)
[26] Görller-Walrand Ch and Binnemans K 1998 *Handbook on the Physics and Chemistry of Rare Earths* vol 25 (Amsterdam: North-Holland) chapter 167
[27] Binnemans K, De Leebeeck H, Görller-Walrand C and Adam J L 1999 *Chem. Phys. Lett.* **303** 76
[28] Tanabe S 2005 Development of rare-earth doped fiber amplifiers for broad band wavelength division multiplexing telecommunication *Photonics Based on Wavelength Integration and Manipulation* Books 2 (Tokyo: IPAP) pp 101–12
[29] Brocklesby W S 1993 *Annu. Rev. Mater. Sci.* **23** 193
[30] Lei G, Anderson J E, Buchwald M I, Edwards B C and Epstein R I 1998 *Phys. Rev.* B **57** 7673
[31] Bigot L, Choblet S, Jurdyc A-M, Jacquier B and Adam J L 2004 *J. Opt. Soc. Am.* B **21** 307
[32] Inoue H, Soga K and Makishima A 2003 *J. Non-Cryst. Solids* **325** 382
[33] Inoue H, Soga K and Makishima A 2002 *J. Non-Cryst. Solids* **298** 270
[34] Inoue H, Soga K and Makishima A 2002 *J. Non-Cryst. Solids* **306** 17
[35] Balda R, Fernández J, Eilers H and Yen W M 1994 *J. Lumin.* **59** 81
[36] Guy S, Bigot L, Vasilief I, Jacquier B, Boulard B and Gao Y 2004 *J. Non-Cryst. Solids* **336** 165
[37] Piątkowski D 2007 *J. Non-Cryst. Solids* **353** 1017
[38] Piątkowski D, Wiśniewski K, Koepke Cz and Naftaly M 2008 Excited state absorption spectroscopy of Nd^{3+} activated fluoroaluminate glass—experiment and simulation *Opt. Mater.* at press

[39] Henderson B and Imbush G F 1989 *Optical Spectroscopy of Inorganic Solids* (Oxford: Clarendon)
[40] de Sousa D F, Peters V, Huber G, Toncelli A, Parisi D and Tonelli M 2003 *Appl. Phys.* B **77** 817
[41] Wnuk A, Kaczkan M, Frukacz Z, Pracka I, Chadeyron G, Joubert M-F and Malinowski M 2002 *J. Alloys Compounds* **341** 353
[42] Joubert M-F 1999 *Opt. Mater.* **11** 181